AD-A048 885 AIR FORCE INST OF TECH WRIGHT-PATTERSON AFB OHIO SCH--ETC F/G 7/4
FURTHER SHOCK TUBE KINETIC STUDIES OF MONOMETHYLAMINE.(U)
DEC 77 J C WERT

UNCLASSIFIED AFIT/GEP/AA/77D-1 NL

| OF |
AD
A048 885

END
DATE
FILMED
2-78
DDC

(1)

FURTHER SHOCK TUBE KINETIC STUDIES OF MONOMETHYLAMINE

THESIS

AFIT/GEP/AA/77D-1 John C. Wert III
Captain USAF

AFIT/GEP/AA/77D-1

FURTHER SHOCK TUBE KINETIC STUDIES OF MONOMETHYLAMINE

THESIS

Presented to the Faculty of the School of Engineering
of the Air Force Institute of Technology
Air University

in Partial Fulfillment of the
Requirements for the Degree of
Master of Science

by

John C. Wert III
Captain USAF

Graduate Engineering Physics

December 1977

(See 1473)

Preface

This thesis is the second in a series of theses which study the route by which organo-nitrogen compounds ultimately form NO_x pollutants. Since petroleum based fuels are getting more scarce and expensive, fuels derived from shale oil and coal look very promising. If the reaction mechanism for the NO_x pollutant formation can be understood, the effects of the inherently high nitrogen content of these alternate fuels may be reduced or eliminated.

The analysis of the pyrolytic decomposition of monomethylamine was performed using infrared emission and shock tube techniques. The activation energies and frequency factors for the decomposition of monomethylamine and the formation of ammonia were determined. Several models for the reaction have been proposed and a determination of a most probable mechanism was possible.

I feel very privileged to have worked in this particular area of research. It has encompassed electronics, gas dynamics, engineering physics, chemical kinetics, computers, and photography, and has contributed greatly to the broadening of my engineering background.

I want to express my deep appreciation for my thesis advisor and instructor, Dr. Ernest A. Dorko, without whose patience, knowledge, and guidance this research would not have been completed. I wish to thank the following people for their help on my thesis: John Parks and Leroy Cannon of AFIT for their technical assistance in maintaining the shock tube equipment; William Baker of AFIT who kept me well stocked with film and other essential supplies; Carl Shortt of the AFIT shop for the excellent machining and parts fabrication. I would also like to thank Drs. George John and William Elrod and Capt. Tom Rosford who served on my thesis committee and provided useful guidance and criticism.

To my wife, Liz, and my children I offer special thanks for your support, understanding, and encouragement during this period.

John C. Wert III

Contents

List of Figures

List of Tables

Abstract

The pyrolytic decomposition of monomethylamine was studied as a first step toward modeling the route by which NO_x pollutants are formed from nitrogen rich compounds such as coal and shale oil. The decomposition of dilute mixtures of monomethylamine in argon was accomplished using shock tube techniques. Kinetic measurements for the decomposition occurring behind the reflected shock were made by means of infrared measurements. Emissions at 3.375 μm due to monomethylamine and 2.886 μm due to ammonia were observed. The total gas concentration behind the reflected shock ranged from 15.32 to 114.7 micromoles/cc. The temperature range was 1275 to 2400 ^{o}K and the total pressure ranged from 1 to 10 atmospheres. The values for the Arrhenius parameters for the decomposition of monomethylamine and the formation of ammonia were determined using a least squares analysis. The high pressure Arrhenius expression for the decomposition is $k = 10^{10.84} e^{-48,150/RT}$. It was discovered that the rate of ammonia formation was one-half the rate of monomethylamine decomposition. The most probable reaction mechanism was determined to be C-N bond scissure followed by a radical chain to produce ammonia, methane, hydrogen cyanide, and hydrogen.

FURTHER SHOCK TUBE KINETIC STUDIES OF MONOMETHYLAMINE

I. Introduction

Background

The continued depletion of petroleum-based fuels makes the consideration of useable alternate fuels, such as those from coal and shale oil, necessary. One of several problems encountered with these fuels is their very high content of organo-nitrogen compounds, typically 0.3 to 2% by weight (Ref 19:3) compared to less than 0.01% for petroleum-based fuels (Ref 6:32). During combustion these compounds produce excessive amounts of NO_x pollutants, 140% more than petroleum-based fuels (Ref 11:5). The symbol NO_x is used to designate the three nitrogen oxides; NO, NO_2, and N_2O_3, which are usually formed during combustion (Ref 2,3). These NO_x pollutants, when emitted from aircraft gas turbines, will eventually participate in smog formation in the lower atmosphere and could possibly have detrimental effects on the stratospheric ozone layer (Ref 3).

As a direct result of the Climatic Impact Assessment Program (CIAP), the Department of Transportation has recommended that accelerated combustion research efforts aimed at substantial reductions in aircraft NO_x emissions be undertaken. Since it is projected that JP4 and JET A fuels will be obtained from coal and shale oil in the near future (Ref 3), the Air Force is also interested in reducing the pollutants formed by their combustion.

Because the physical and chemical phenomena that govern the formation and emission of aircraft gas turbine pollutants are complex and not well understood, the scientific base from which firm conclusions and problem approaches might be drawn is insufficient to support future efforts to

reduce such pollutants. It is therefore necessary to first understand the reaction mechanisms by which organo-nitrogen compounds form NO_x pollutants, called fuel NO_x. Then, once these reaction mechanisms are determined, the pollutant-forming step(s) may be eliminated or slowed down.

It has been known for some time that the fixation of atmospheric nitrogen is the chief source of NO_x pollutants from combustion of petroleum-based fuels. This reaction is believed to proceed according to the Zeldovich mechanism, which is as follows:

$$O_2 + M \rightarrow 2O + M$$

$$O + N_2 \rightarrow NO + N$$

$$N + O_2 \rightarrow NO + O$$

It is also known that the formation of thermal NO_x by this mechanism can be suppressed by operating at low temperatures. However, the reactions which lead to fuel NO_x pollutants from organo-nitrogen compounds occur much more readily at combustion temperatures. This knowledge has prompted the study of the mechanistic route by which a model organo-nitrogen compound ultimately forms NO_x. The compound chosen as a suitable model is monomethylamine (MMA) (Ref 14).

Research Objectives

This thesis presents a further shock tube kinetic study of the decomposition of monomethylamine in argon, which is the first step towards modeling the route by which organo-nitrogen compounds form NO_x pollutants. The reaction was studied through the use of infrared emission detection and proven shock tube techniques (Ref 9). The Arrhenius parameters for the decomposition of MMA and the formation of ammonia at several different total gas concentrations were to be calculated. The

nature of any other products and a dominant reaction pathway for the decomposition of monomethylamine were to be determined.

II. Theory

Kinetics and Mechanism

A unimolecular reaction can be represented by the elementary equation

$$A \rightarrow \text{Products} \tag{1}$$

and the rate of disappearance of A is

$$-\frac{d[A]}{dt} = k[A] \tag{2}$$

which is a 1^{st} order reaction in A. Separation of variables and integration yields

$$\frac{[A]}{[A_o]} = e^{-kt} \tag{3}$$

which means that in a 1^{st} order reaction the concentration of [A] decreases exponentially with time.

Before a unimolecular reaction can take place, the reacting molecule must acquire sufficient energy to cause the reaction to occur. For a thermal reaction, the energy is acquired through molecular collisions. Lindemann made the original suggestion that a unimolecular reaction could take place under the influence of collisions, and Hinshelwood showed that the energy stored by a molecule was a function of the internal degrees of freedom (Ref 16:20). The basic Hinshelwood-Lindemann equations are

$$A + M \xrightarrow{k_a} A^* + M \tag{4}$$

$$A^* + M \xrightarrow{k_d} A + M \tag{5}$$

$$A^* \xrightarrow{k_e} B \tag{6}$$

where A is the reactant, A* is the excited molecule, B is the product, M is either reactant or an added inert gas, and k_a, k_d, and k_e are the rate constants (Ref 21:119) for activation, deactivation, and reaction respectively.

The Hinshelwood modification to the Lindemann theory showed that there was a delay between activation and reaction to form products. The energy must be redistributed among the vibrational degrees of freedom before enough energy is placed into one or at most a few vibrational modes to cause reaction. This time delay permits the deactivation of the energized molecule to take place, Eq (5) (Ref 16:20).

By use of the steady state approximation for A* (Ref 21:19), the rate of disappearance of A becomes

$$-\frac{d[A]}{dt} = \frac{k_a k_e [A][M]}{k_d[M] + k_e} = k_{uni}[A] \tag{7}$$

where $k_{uni} \equiv \frac{k_a k_e [M]}{k_d[M] + k_e}$, and is the experimental 1^{st} order rate constant. These equations show that k_{uni} is a function of $[M]$ and will therefore be a function of the total pressure. There are two limiting cases which permit simpler expressions for k_{uni}.

In the high pressure limit, $k_d[M] \gg k_e$, and

$$k_{uni} = \frac{k_a k_e}{k_d} = k_\infty \tag{8}$$

and the rate equation then becomes

$$-\frac{d[A]}{dt} = k_\infty[A] \tag{9}$$

which is 1^{st} order in A and independent of the total pressure. This rate of reaction is so low compared with deactivation, that the equilibrium fraction of $\frac{[A^*]}{[A]} = \frac{k_a}{k_d}$ is maintained. The rate constant, k_∞, is therefore the product of the rate for spontaneous decomposition and the fraction of molecules which are activated.

In the low pressure limit, $k_e \gg k_d[M]$, and

$$k_{uni} = k_a[M] \tag{10}$$

and the rate equation becomes

$$-\frac{d[A]}{dt} = k_a[A][M] \tag{11}$$

which is 1st order in A and linearly dependent on the total pressure. The above two limiting cases determine that the power dependence of k_{uni} on [M] will be between 0 and 1.

Monomethylamine, CH_3NH_2, was chosen for study because it and the initially assumed products have at least one distinct and non-overlapping infrared spectral region. MMA is a stable, readily available, gaseous amine, analogous to ethane, which is a hydrocarbon whose combustion has been previously studied.

Three distinct decomposition reaction mechanisms may be reasonably postulated for the decomposition. It should be noted that the first step in the three different postulated reactions is a unimolecular decomposition, however, the reaction pathway is significantly different in each case (Fig 1). After the first step, there are substantial differences in the subsequent reaction steps and in the products which are formed.

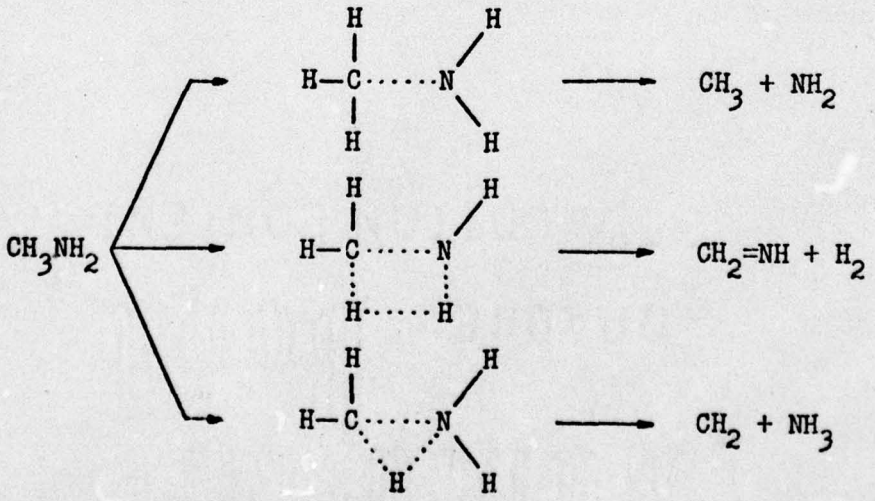

Fig 1. Unimolecular Decomposition Mechanisms

In initial studies by Hidaka, Saito, and Yamamura (Ref 12), they postulated scissure of the CN bond to form the methyl and amide radicals followed by a radical chain reaction. The mechanism postulated is as follows:

$$CH_3NH_2 \rightarrow CH_3 + NH_2 \tag{12}$$

$$CH_3 + CH_3NH_2 \rightarrow C_2H_6 + NH_2 \tag{13}$$

$$CH_3 + CH_3NH_2 \rightarrow CH_4 + CH_2NH_2 \tag{13a}$$

$$NH_2 + CH_3NH_2 \rightarrow CH_3 + N_2H_4 \tag{14}$$

$$2CH_3 \rightarrow C_2H_6 \tag{15}$$

Application of the steady state approximation to the rate equations for $[CH_3]$ and $[NH_2]$, yielded the following rate expression for the disappearance of MMA

$$-\frac{d[CH_3NH_2]}{dt} = 2\left\{k_1 + k_2\left(\frac{2k_1[CH_3NH_2]}{k_4}\right)^{\frac{1}{2}}\right\}[CH_3NH_2] \tag{16}$$

If $k_1 \ll k_2\left(\frac{2k_1[CH_3NH_2]}{k_4}\right)^{\frac{1}{2}}$, then the rate equation reduces to

$$-\frac{d[CH_3NH_2]}{dt} = 2k_2\left(\frac{2k_1}{k_4}\right)^{\frac{1}{2}}[CH_3NH_2]^{\frac{3}{2}} \tag{17}$$

This expression indicates a 3/2 order power dependence of the reaction on monomethylamine concentration.

The CN bond scissure may also be considered analogous to the unimolecular bond scissure of ethane followed by a radical chain mechanism. A recent single-pulse shock tube study in conjunction with vapor phase chromatobraphy (Ref 4) details the decomposition of ethane. The data of this report correlates well with the assumption of unimolecular reaction kinetics for the initial step. A similar reaction sequence for MMA (Appendix A) would proceed as follows:

$$CH_3NH_2 \rightarrow CH_3 + NH_2 \quad (18)$$

$$CH_3 + CH_3NH_2 \rightarrow CH_4 + CH_2NH_2 \quad (19)$$

$$CH_2NH_2 \rightarrow CH_2{=}NH + H \quad (20)$$

$$H + CH_3NH_2 \rightarrow H_2 + CH_2NH_2 \quad (21)$$

$$H + CH_3 \rightarrow CH_4 \quad (22)$$

By use of the steady state approximation the rate expression for the disappearance of MMA is

$$-\frac{d[CH_3NH_2]}{dt} = \frac{3}{2}k_1[CH_3NH_2] + \frac{k_2k_4}{k_5}[CH_3NH_2]^2 \quad (23)$$

which is a combination of 1st and 2nd order reactions with respect to MMA.

The final CN bond scissure reaction (Appendix B) to be postulated is as follows:

$$CH_3NH_2 \rightarrow CH_3 + NH_2 \quad (24)$$

$$CH_3 + CH_3NH_2 \rightarrow CH_4 + CH_2NH_2 \quad (25)$$

$$CH_3 + CH_2NH_2 \rightarrow CH_4 + CH_2{=}NH \quad (26)$$

$$NH_2 + CH_3NH_2 \rightarrow NH_3 + CH_2NH_2 \quad (27)$$

$$NH_2 + CH_2NH_2 \rightarrow NH_3 + CH_2{=}NH \quad (28)$$

$$CH_2{=}NH \rightarrow H_2 + HCN \quad (29)$$

Also by use of the steady state approximation, the rate expression for the disappearance of MMA is

$$-\frac{d[CH_3NH_2]}{dt} = 2k_1[CH_3NH_2] \quad (30)$$

which is a 1st order reaction in MMA.

The second reaction mechanism which can reasonably be postulated involves the formation of a long-lived imine intermediate from which HCN is then formed.

$$CH_3NH_2 \rightarrow CH_2{=}NH + H_2 \quad (31)$$

$$CH_2{=}NH \rightarrow HCN + H_2 \quad (32)$$

This mechanism was proposed recently by Smith and Sawyer (Ref 17) to explain the decomposition of MMA mixed with helium in a flow reactor. They found methane, ammonia, nitrogen, traces of hydrogen cyanide, and solid hexamethylene-tetramine, 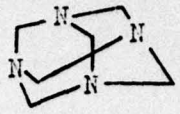 , which they postulate is produced from the imine intermediate. At higher temperatures the imine intermediate breaks down to form HCN as shown in Eq (32). The experimentally determined rate expression is

$$-\frac{d[CH_3NH_2]}{dt} = k[CH_3NH_2]^{.28} \tag{33}$$

The last reaction mechanism to be postulated is as follows:

$$CH_3NH_2 \rightarrow CH_2 + NH_3 \tag{34}$$

$$2CH_2 \rightarrow CH_2{=}CH_2 \tag{35}$$

There is some evidence to show that this mechanism can reasonably be expected to occur. A recent shock tube study by Meyer and Wagner (Ref 13) on hydrazine presents evidence for hydrogen transfer as in Eq (36). This

$$N_2H_4 \rightarrow NH_3 + NH \tag{36}$$

reaction would lead to formation of a nitrene.

Shock Tube Studies of Reaction Rates

Shock tubes have been used extensively in chemical kinetics (Ref 1). A technique used successfully in the past (Ref 9) combines the detection of infrared emission with shock tube techniques to study the rates of chemical changes in situ. This method consists of monitoring the infrared emission at a very specific wavelength to determine if there is a decrease of reactant or an increase of product. Table I shows the wavelength of infrared radiation characteristic of the reactant and products which could conceivably be present during the decomposition of monomethylamine (Ref 15).

Table I

Reactant/Products and Infrared Wavelengths

Molecule	Wavelength (μm)
CH_3NH_2	3.40
C_2H_6	6.5-7.0
HCN	7.25
CH_2=NH	6.0
NH_3	2.85
CH_4	7.7
CH_2=CH_2	5.25

For example, if there is an increase with time in emission at 2.85 μm, then ammonia, NH_3, is forming. If no emission were detected at 5.25 μm, then no ethylene, CH_2=CH_2, is forming. Based upon the information thus obtained, a plausible mechanism can be postulated and the reaction rate constants be determined (Ref 8).

In addition to the *in situ* infrared emission technique, the reaction mechanism can be studied through the use of a single-pulse shock followed by product analysis by vapor phase chromatography (Ref 1,7).

III. Experimental

The shock tube used in these experiments was fabricated from 3 inch i.d. stainless steel (SS304) tubing with 3/8 inch walls. The tubing was shaped on a mandrel to produce a cross section at the reaction end which had two parallel, flat sides with a width of about 1 inch. The flat sides made it convenient to attach instrumentation and the absence of corners minimized boundary layer effects. The tube was 23 feet long with a 16 foot driver and a 7 foot driven section. The tube has been described more fully elsewhere (Ref 14).

A 1% MMA test gas mixture was prepared from MMA (98.0% pure) and argon (99.995% pure), both purchased from Matheson Gas Products. Shock parameters were calculated for the specific gas mixtures from the initial shock velocity assuming frozen chemistry. The heat capacities for MMA were obtained from the data contained in NASA Program 273 and from thermodynamic tables (Ref 16). The total gas concentration behind the reflected shock ranged from 15.32 to 114.7 micromoles/cc. The temperature range was 1275 to 2400 ^{o}K and the total pressure ranged from 1 to 10 atmospheres. A total of 200 gas samples were investigated in the shock tube and the results were used in the analysis.

Kinetic measurements were obtained for the decomposition occurring behind the reflected shock by detection of infrared (IR) emission through two CaF_2 windows placed in the opposing flat walls of the shock tube 12 mm from the end flange of the driven section. These windows were fabricated by the Industrial Lens Company and mounted in stainless steel adapters. The window surfaces were made flat to one-half wavelength and parallel to ten seconds of arc. Three distinct advantages were apparent when using CaF_2 windows: CaF_2 is transparent in the visible region, permitting visual

focusing of the alignment coil (Ref 14) on the pinhole; it is not transparent above 8 μm, thereby acting as a cutoff filter; and it transmits 15% more radiation than Irtran II, for example, in the region of interest.

The IR emission from the shock tube was simultaneously monitored by two separate optical systems. A system employing an indium-antimonide (InSb) detector was used to observe emission in the range from 1-5 μm and a system employing a mercury-cadmium-telluride (HgCdTe) detector was used to observe emission in the range from 6-8 μm.

The InSb system consisted of the focusing lens, pinhole/filter assembly, and detector (Fig 2). The lens was made from CaF_2 and had a

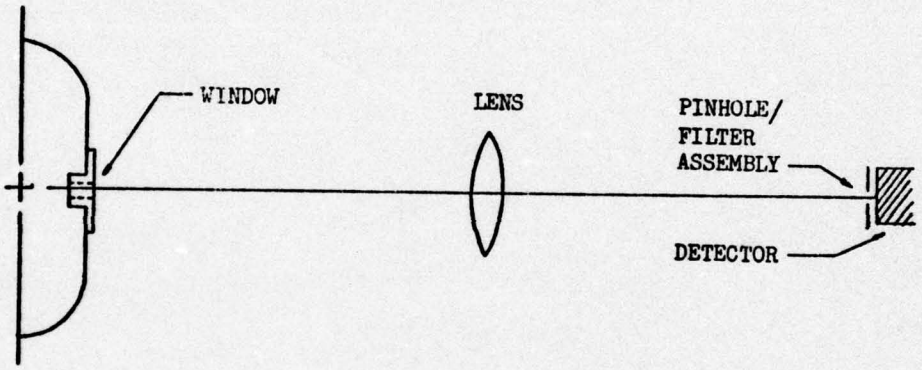

Fig 2. InSb Optical System

focal length of 25 cm. The InSb detector was a Barnes Engineering type J-10 (liquid nitrogen cooled) used in conjunction with a Perry Associates Preamplifier Model Number 720.

The HgCdTe system consisted of first-surface gold-coated mirrors, pinhole/filter assembly, and detector (Fig 3). The gold-coated mirrors were used to minimize absorption losses. The HgCdTe detector was a Santa Barbara Research Center (SBRC) Model 127 (liquid nitrogen cooled) and was used in conjunction with a SBRC Model A120 Preamplifier.

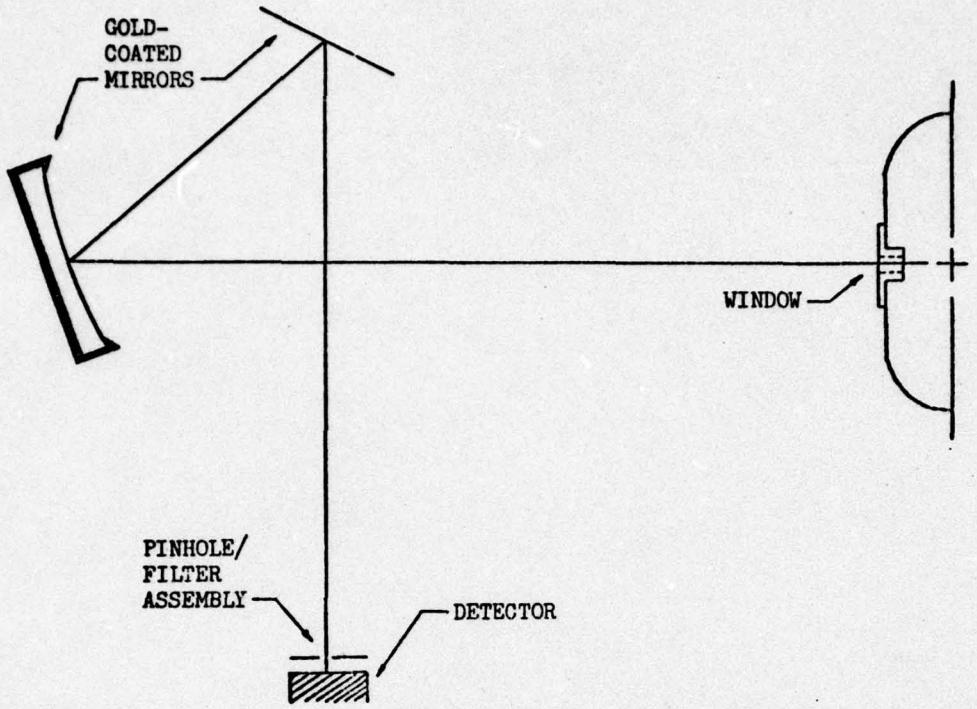

Fig 3. HgCdTe Optical System

The output signal from each detector was fed through its own pre-amplifier and then into the upper beams of separate Tektronix Type 551 Dual-Beam Oscilloscopes. These oscilloscopes were triggered by a time-delayed signal from a Tektronix Type 549 Oscilloscope which was triggered by an output signal from the heat gauge at the last velocity station (Ref 14). A signal originating from a Tektronix Type 180A Time Mark Generator was fed into the lower beam of each 551 oscilloscope for use as a calibrated time base. Photographs of the oscilloscope traces were made with Tektronix Series 125 Cameras with Polaroid Series 40 Camera Backs.

A series of experiments was run in which a 3.375 μm filter (FWHM of 0.20 μm), from Optical Coatings Laboratory, was inserted in the pinhole/

filter assembly of the InSb detector system in order to monitor the decomposition of MMA. A typical oscillogram of MMA decomposition is shown in Fig 4.

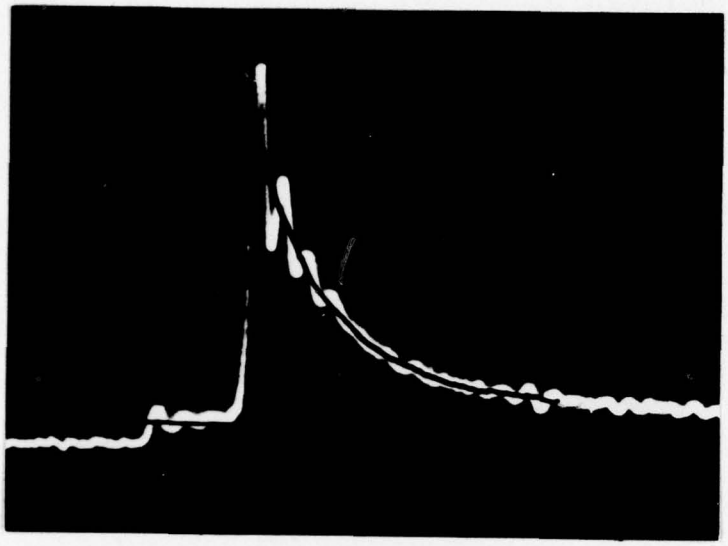

T = 1678 ^{o}K
P = 4.58 Atm
[M] = 33.2 μmoles/cc
Horizontal = 50 μsec/cm
Vertical = 5 mv/cm
Time Marks = 10 μsec

Fig 4. Oscillogram for the Decomposition of MMA. (1% MMA in Argon)

Numerical data was obtained from each oscillogram by measuring the relative intensity versus time. The procedure used was as follows. A reference baseline, which was an extension of the zero intensity portion of the trace obtained prior to the arrival of the reflected shock, was drawn on the oscillogram. Next a smooth curve was drawn through the trace obtained after passage of the reflected shock wave. The initial time was chosen as the time-mark coincident with the maximum intensity of the oscillogram. The relative intensity was then measured with a traveling microscope and digital voltmeter as described in Ref 14. A plot of the logarithm of the relative intensity versus time yielded a straight line, the negative slope of which was defined to be k_{uni}.

Another series of experiments was run in which a 2.886 μm filter (FWHM of 0.22 μm), from Optical Coatings Laboratory, was inserted in the

pinhole/filter assembly of the InSb detector system to monitor the formation of ammonia, NH_3. A typical oscillogram is shown in Fig 5.

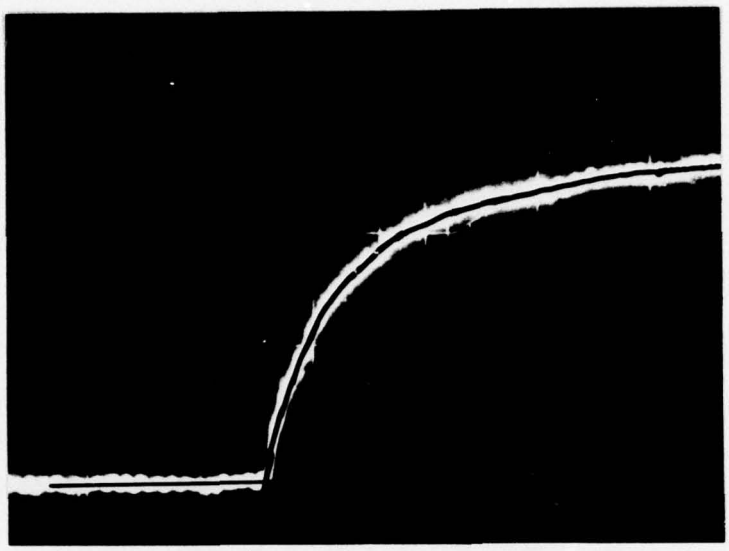

T = 1635 °K
P = 4.41 Atm
[M] = 32.9 μmoles/cc
Horizontal = 100 μsec/cm
Vertical = 1 mv/cm
Time Marks = 10 μsec

Fig 5. Oscillogram for the Formation of NH_3.
(1% MMA in Argon)

Inasmuch as the emission intensity is increasing with time, a slightly different method of data reduction was used.

The baseline was drawn through the zero intensity portion of the oscillogram and a smooth curve was drawn through the remainder of the trace. This curve was then extended towards infinity and a line tangent to the curve at this "infinite" point was constructed back to time equal to zero. This line represented the maximum intensity (I_{max}) for each oscillogram. The relative intensity was then calculated by use of the following formula (Appendix C)

$$I_{rel} = \frac{I_{max} - I_{measured}}{I_{max}} \qquad (37)$$

where $I_{measured}$ is the trace intensity at any time between 0 and infinity.

In addition to the two series of tests described, another series was run with a 5.230 μm filter (FWHM of 0.36 μm), from Optical Coatings Labora-

tory, inserted in the pinhole/filter assembly of the InSb detector system. A typical oscillogram is shown in Fig 6. Because of the complexity of the processes which gave rise to the oscillogram, no simple data reduction and analysis were possible.

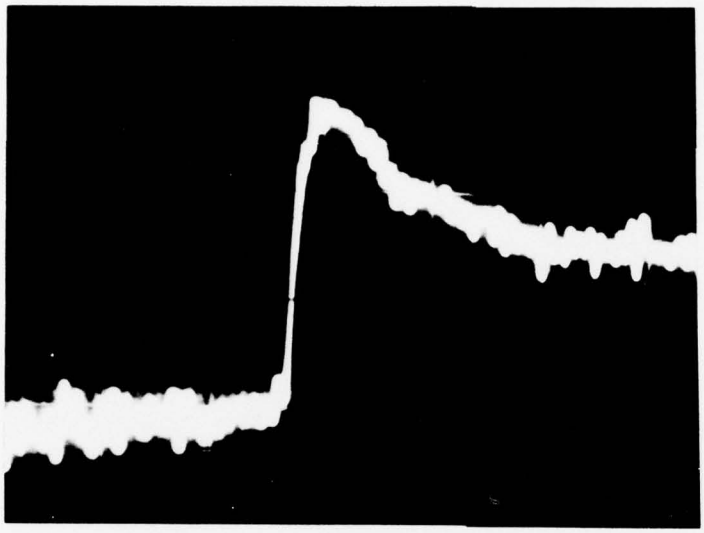

T = 1617 ^{o}K
P = 4.33 Atm
[M] = 32.6 μmoles/cc
Horizontal = 100 μsec/cm
Vertical = 2 mv/cm
Time Marks = 10 μsec

Fig 6. Oscillogram for the Emission at 5.230 μm. (1% MMA in Argon)

Attempts to obtain useable data with the HgCdTe detector system were unsuccessful. While the detector system was able to detect a signal from the alignment coil, the IR emission from the shock tube during the shock was undetectable apparently due to detector sensitivity. The filters used were 7.597 μm (FWHM of 0.06 μm), 7.300 μm (FWHM of 0.21 μm), and 5.230 μm (FWHM of 0.36 μm), all purchased from Optical Coatings Laboratory.

IV. Results

To test the compatibility of the data reduction process performed previously (Ref 14) and presently, a series of experiments in which the total gas concentration was held at 53.04 micromoles/cc was performed. This data was numerically reduced as described previously and the activation energy, E_a, and frequency factor, A, as calculated using a least squares technique (Ref 14), were within one sigma between researchers. The series of tests at [M] = 83.73 micromoles/cc, as reported by Pchelkin (Ref 14), was numerically reduced again from the oscillograms and the calculated values for E_a and A were within one sigma between researchers. The data thus obtained is also included in this thesis.

The Arrhenius plots (Log k_{uni} vs 1/T) for the decomposition at five different total gas concentrations are shown in Fig 7. The curves were obtained by a least squares analysis of the data (Ref 14). It can be noticed that there is somewhat of a fanning out of the curves. This effect is expected if the system obeys the Hinshelwood-Lindemann theory. The reason for this is that as the pressure is increased the activation energy of the reaction (and therefore the slope of the Arrhenius plot) increases until the high pressure limit is reached. Notice that this fan effect is most pronounced at low pressure and is hardly noticeable as the system reaches its high pressure limit.

In addition to the change in slope, the separation between curves decreases as the pressure is increased. This result is as expected with a Hinshelwood-Lindemann reaction. At a temperature of 1667 ^{o}K the logarithmic difference between the two lowest pressure curves is 0.197 while the logarithmic difference between the two highest pressure curves is 0.044.

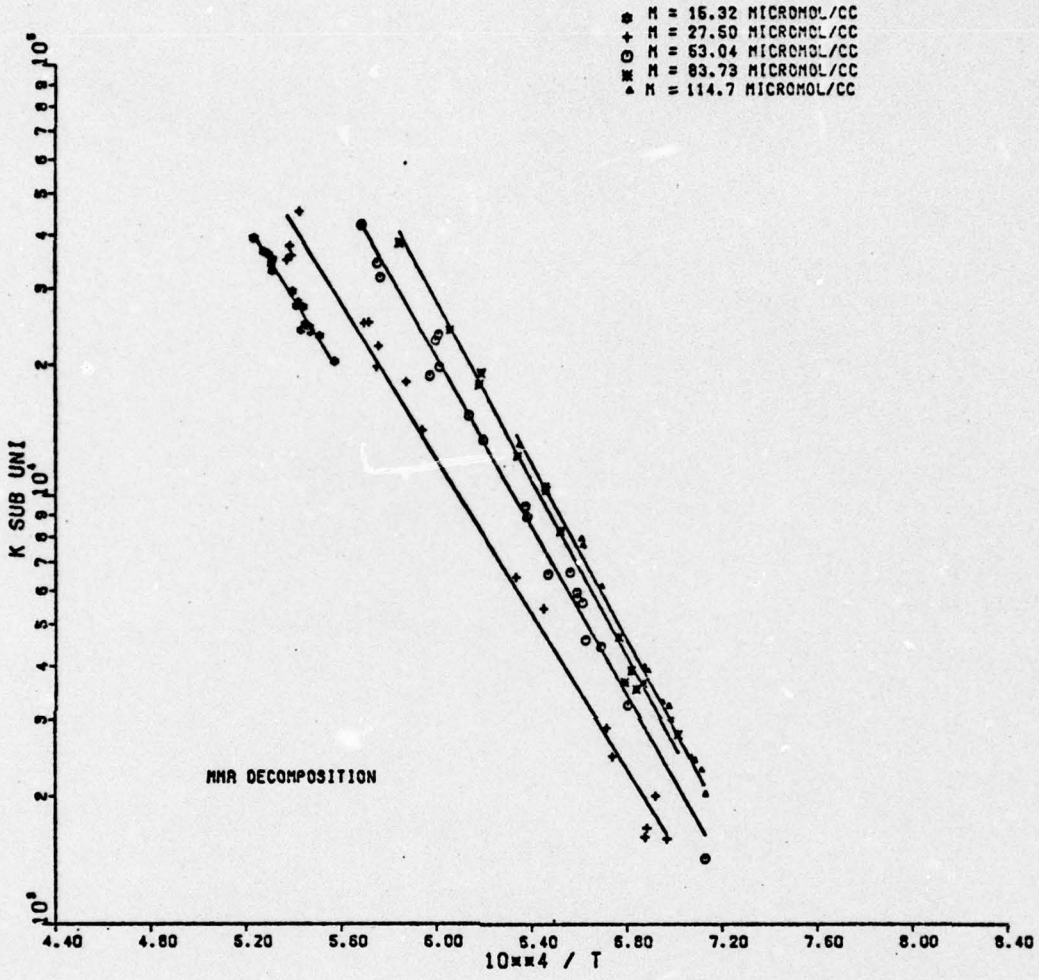

Fig 7. Semi-Logarithmic Plots of k_{uni} vs 1/T for the Decomposition of MMA

These differences correspond to a total concentration power dependence of 0.78 and 0.32 at the low and high pressure experimental extremes respectively. The values of the Arrhenius parameters for MMA decomposition are given in Table II.

Table II

Arrhenius Parameters for Monomethylamine Decomposition

[M] (micromoles/cc)	E_a (kcal/mole)	Log A (cc/mole sec)
15.32	40.79 ± 0.61	9.27 ± 0.14
27.50	41.17 ± 2.25	9.48 ± 0.52
53.04	44.88 ± 1.62	10.20 ± 0.37
83.73	47.07 ± 1.46	10.62 ± 0.33
114.7	47.39 ± 0.71	10.70 ± 0.16
low pressure	35.14	13.50
high pressure	48.15	10.84

Figure 8 displays logarithmic plots of k_{uni} vs P for various constant temperatures. The data for these plots was obtained from the Arrhenius parameters in Table II. As shown in Section II at the high pressure limit in the Hinshelwood-Lindemann mechanism the theoretical variation of k_{uni} with concentration, or from the ideal gas law, pressure, is equal to zero. It is evident that the experimental variation of k_{uni} with concentration is approaching this zero limit. At the low pressure limit the Hinshelwood-Lindemann mechanism predicts a linear dependence of k_{uni} on concentration. It can be seen from Fig 8, that as the temperature increases the slopes of the lines approach, but do not reach, one. This indicates that the experimental observations were made in the intermediate to high pressure regime. The low pressure regime was beyond conditions that could be attained in the present experiment. By use of the data points from this figure, the values of the Arrhenius parameters, shown in Table II, for the high pressure regime and for the lowest experimental pressure were calculated.

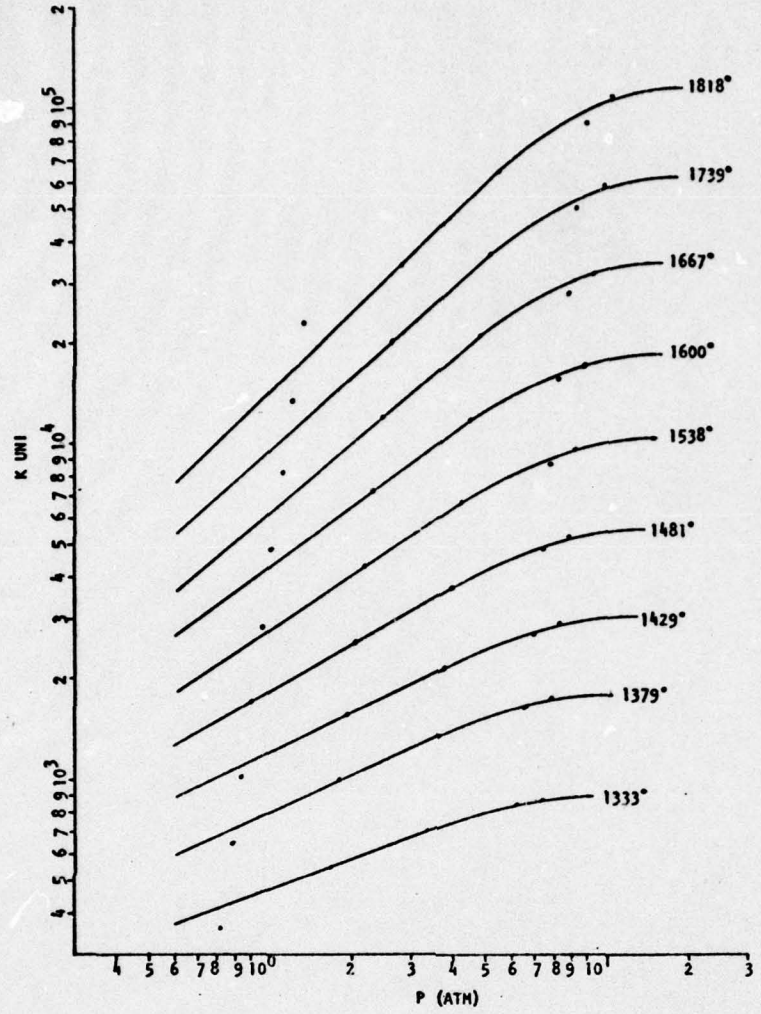

Fig 8. Logarithmic Plots of k_{uni} vs P (atm) at Various Constant Temperatures.

The activation energy, E_a, at low pressure is 13.01 kcal/mole less than E_a at high pressure. This corresponds to a decrease of about 4RT in the temperature range under consideration. This decrease is not as expected from the simple Hinshelwood-Lindemann theory. According to this theory the difference between high and low pressure activation energies is

$$E - E_o = (S-1)RT \qquad (37)$$

where S is a number usually taken to be 2/3 the number of vibrational fundamentals, which for MMA is $\frac{2}{3}(15)$ or 10. Thus an activation energy

difference of about 27 kcal is expected between the high and low pressure regimes. The conclusion from this discussion is that the low pressure regime has not been reached under the experimental conditions used. For a molecule such as MMA with 7 atoms this is not an unexpected result. The low pressure regime for such polyatomic molecules may not occur before the pressure is well below atmospheric (Ref 21:138).

The Arrhenius plots for the formation of NH_3 at different total gas concentrations are shown in Fig 9. The best fit lines obtained by a least

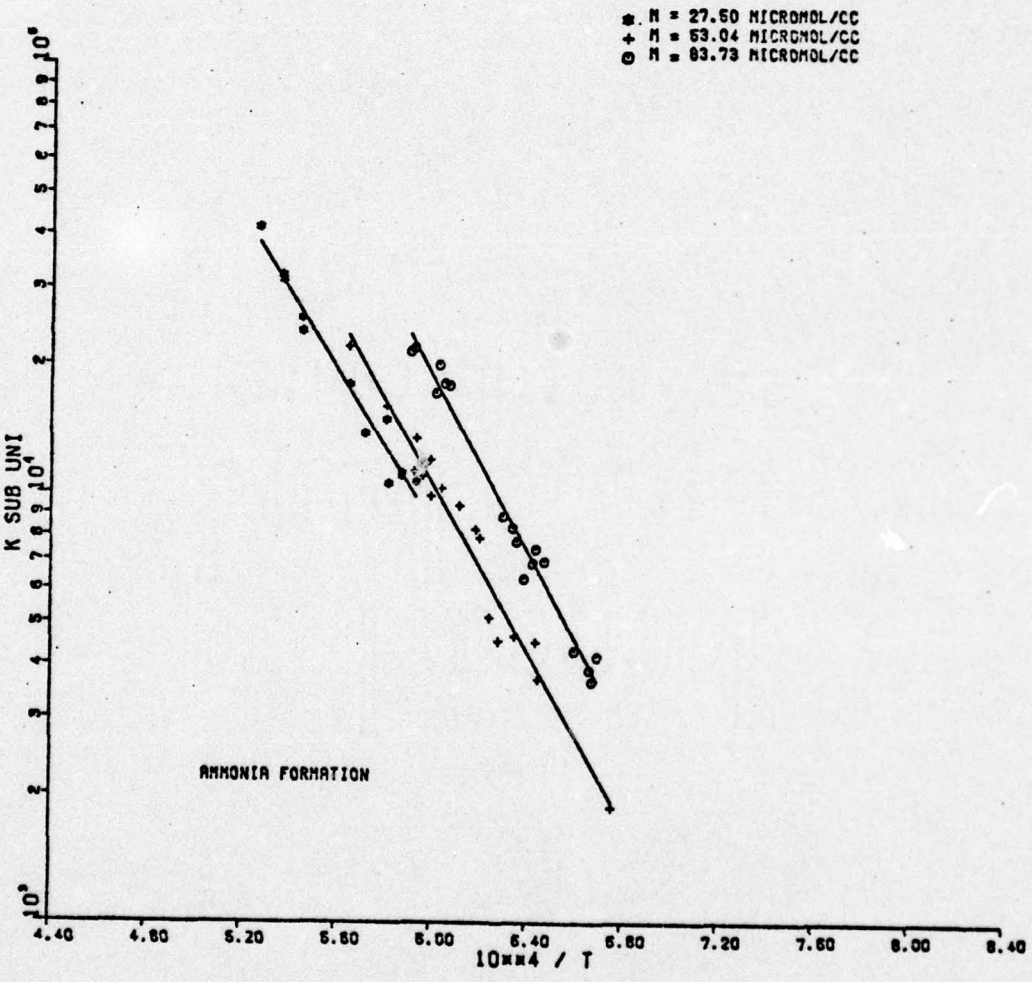

Fig 9. Semi-Logarithmic Plots of k_{uni} vs 1/T for the Formation of NH_3

squares fit, are seen to fan out similarly to those of MMA. The values of the Arrhenius parameters for the formation of ammonia are presented in Table III.

Table III

Arrhenius Parameters for Ammonia Formation

[M] (micromoles/cc)	Ea (kcal/mole)	Log A (cc/mole sec)
27.50	40.75 ± 1.49	9.28 ± 0.34
53.04	44.55 ± 2.09	9.87 ± 0.47
83.73	46.48 ± 1.75	10.37 ± 0.39

The Arrhenius plots for both MMA decomposition and NH_3 formation for different total gas concentrations are shown in Figures 10, 11, and 12.

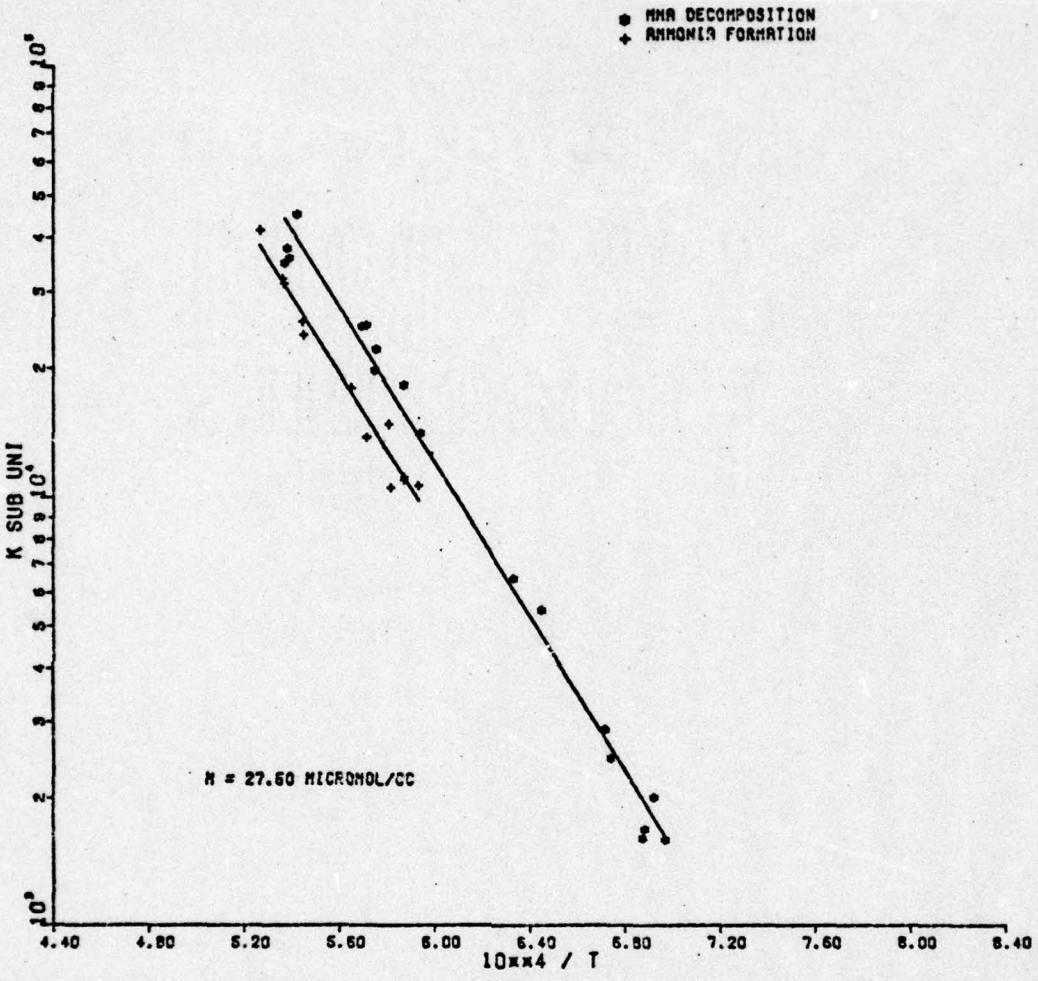

Fig 10. Comparison of Arrhenius Plots for MMA and NH_3. [M] = 27.50 micromoles/cc

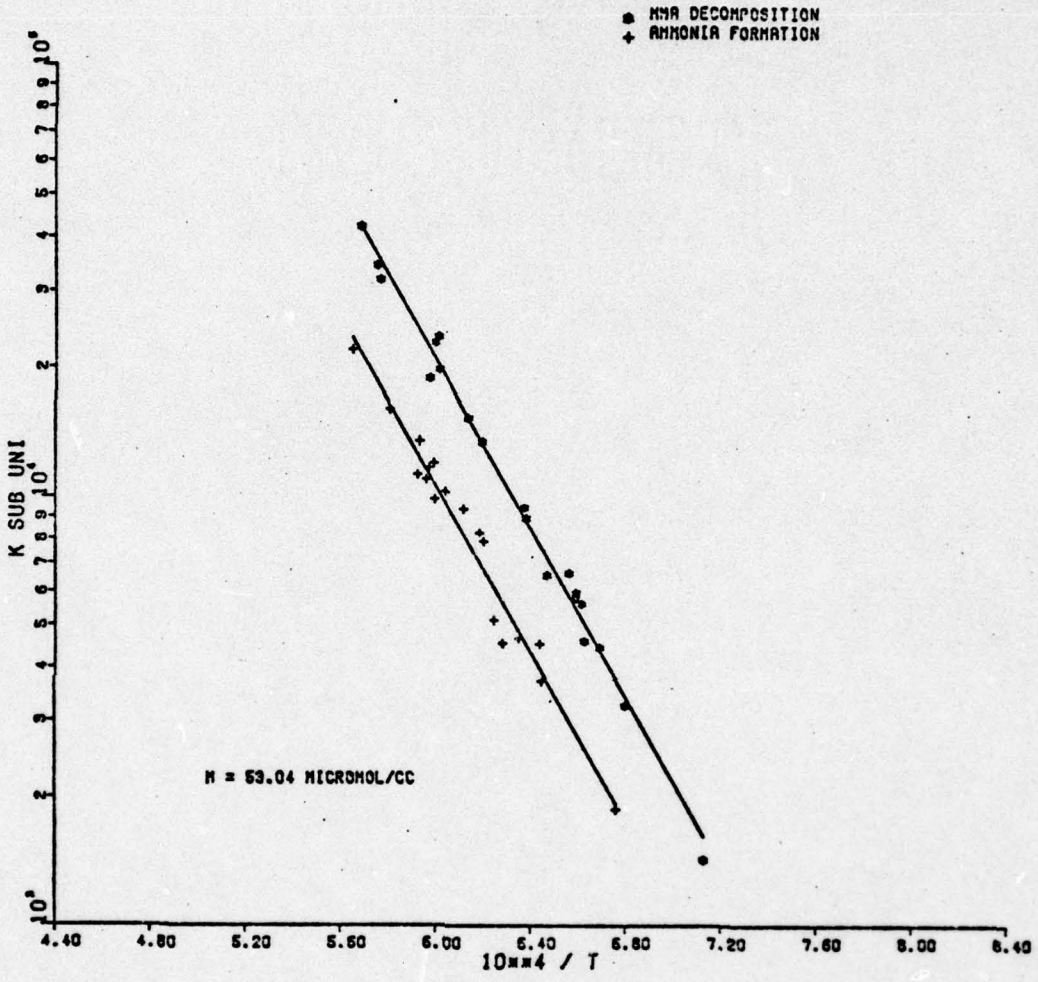

Fig 11. Comparison of Arrhenius Plots for MMA and NH_3. [M] = 53.04 micromoles/cc

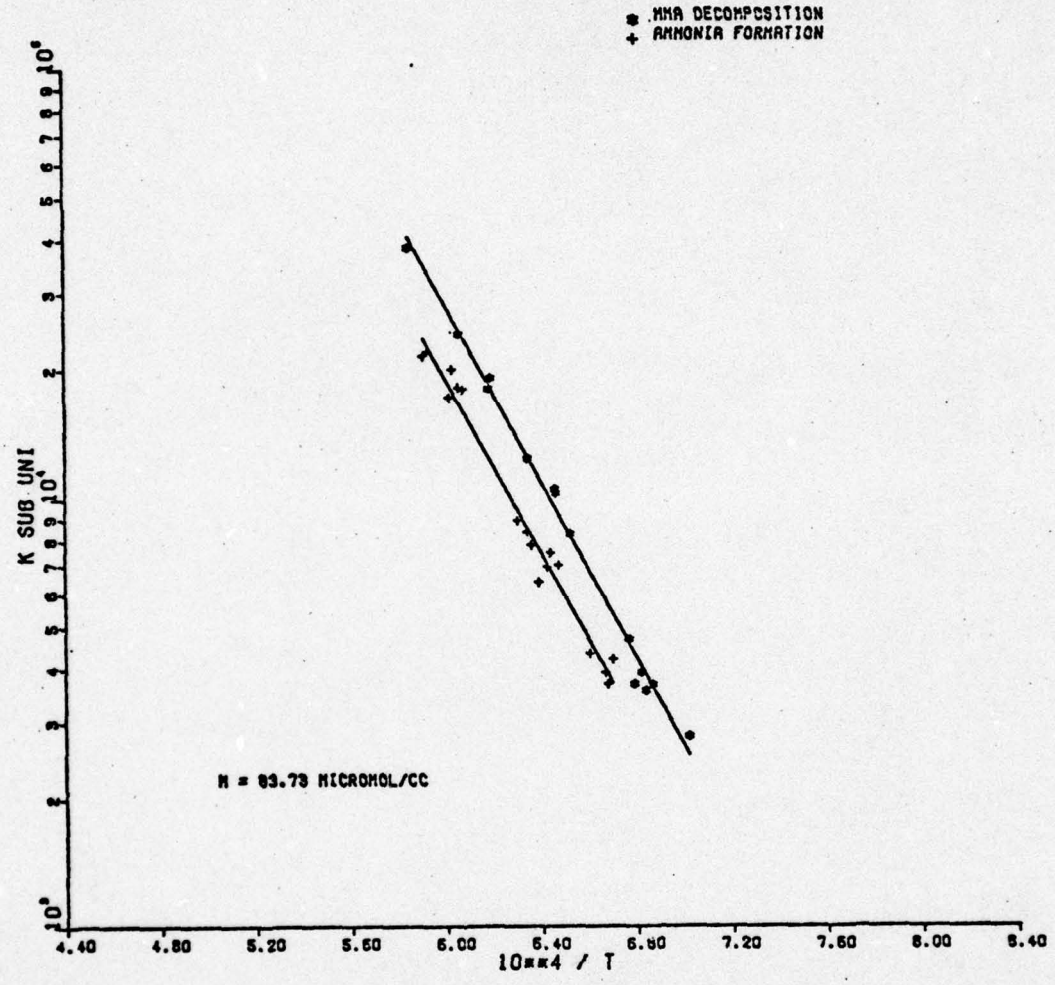

Fig 12. Comparison of Arrhenius Plots for MMA and NH_3. [M] = 83.73 micromoles/cc

V. Discussion

The experimental results need to be discussed in the light of the reasonable mechanisms postulated in Section II. This discussion is an attempt to decide if one of the mechanisms is dominant and if so, which one.

A relationship between MMA and ammonia, one of the products, needs to be established. From Appendix C

$$\alpha = \frac{k}{k'}, \tag{38}$$

where k is the rate constant for MMA decomposition and k' is the rate constant for NH_3 formation. When the values for k and k' from Tables II and III for [M] = 27.05, 53.04, and 83.73 micromoles/cc are substituted into Eq (38), the values for α of 1.58, 2.13, and 1.78 respectively are obtained. If the approximate value of $\alpha = 2$ is substituted into Eq (39) (from Appendix C), then Eq (40) is obtained.

$$\frac{d[NH_3]}{dt} = k'[CH_3NH_2] = \frac{k}{\alpha}[CH_3NH_2] \tag{39}$$

$$\frac{d[NH_3]}{dt} = \frac{k}{2}[CH_3NH_2] \tag{40}$$

When this experimental result is compared with Eq (41) which was obtained from Appendix D

$$\frac{d[NH_3]}{dt} = k_1[CH_3NH_2] \tag{41}$$

the similarity is readily apparent. In this case $k = 2k_1$, which is the result obtained for the derived rate constant for the postulated reaction mechanism in Appendix B. The conclusion is that MMA decomposes at twice the rate at which NH_3 is formed.

In a prior report (Ref 14) it was established that the reaction is first order in MMA concentration. The present results show that the power dependence on total gas concentration varies from 0.32 to 0.78. These two results are strong evidence to eliminate two of the three

postulated radical chain mechanisms. The model proposed by Hidaka, et al, (Ref 12) which is a 3/2 order reaction, is not supported by the established first order dependence although E_a and A are comparable. This first order dependence also does not support the ethane analogous reaction which is a combination of first and second orders. Additional evidence to indicate the dominance of the third postulated radical chain mechanism, if indeed a radical chain does occur, follows.

Table IV

Heats of Formation for Selected Compounds

Compound	ΔH_f (kcal/mole)
CH_4	-17.889
CH_3	34.0
CH_3-CH_3	-20.236
CH_2=CH_2	12.496
CH CH	54.194
NH_3	-11.4
NH_2	47.2
CH_3NH_2	-6.7
CH_3NH	45.4
CH_2=NH	9.02*
HC N	31.2

*Appendix E

(Ref 5)

The following heats of reaction were calculated for several of the postulated reaction steps using the values in Table IV.

① $CH_3NH \rightarrow CH_2{=}NH + H$

$\Delta H_f = 9.02 + 52.104 - (45.4)$

$= +15.724$ kcal/mole

The positive sign indicates endothermicity, which means that energy would have to be added for the step to take place.

② $CH_3NH + CH_3 \rightarrow CH_4 + CH_2{=}NH$

$\Delta H_f = -17.889 + 9.02 - (45.4 + 34.0)$

$= -88.269$ kcal/mole

The negative sign indicates exothermicity, which means that energy is given off and the reaction would occur spontaneously.

③ $CH_3NH + NH_2 \rightarrow NH_3 + CH_2{=}NH$

$\Delta H_f = -11.4 + 9.02 - (45.4 + 47.2)$

$= -94.98$ kcal/mole

Here again the negative sign indicates exothermicity and spontaneity. Since reactions ② and ③ are highly exothermic and reaction ① is endothermic, reactions ② and ③ would be strongly favored over reaction ①. This result would tend to eliminate the ethane analogous decomposition of MMA from consideration.

At this point it should be noted that CH_2NH_2 and CH_3NH have been used interchangeably. This is due to the fact that the activation energies for their formation are 8.7 and 5.7 kcal/mole respectively (Ref 10). There would therefore be no noticeable preference for the formation of one over the other. Another point in favor of the interchangeability is that the bond strengths of C-H and N-H in CH_3NH_2 are 97 (Ref 12) and 92 (Ref 5) kcal/mole respectively.

Regarding the three-center and four-center pathways as shown in Fig 1, the following information needs to be considered. The experimentally determined rate of formation of ammonia

$$\frac{d[NH_3]}{dt} = -\frac{1}{2}\frac{d[CH_3NH_2]}{dt} \tag{42}$$

would preclude the hydrogen transfer mechanism as in Eq (23), the three-center pathway, since that mechanism would require a rate of formation of ammonia of Eq (43)

$$\frac{d[NH_3]}{dt} = -\frac{d[CH_3NH_2]}{dt} \tag{43}$$

Also, the odor of cyanide, which is not formed in the hydrogen transfer reaction, was very noticeable when the shock tube diaphragms were changed between shots.

The four-center mechanism in Fig 1 (Equations 20-21) involves the formation of a long-lived imine and would give as products only hydrogen and hydrogen cyanide. Since ammonia is formed in the present experiment as evidenced by the IR emission at 2.886 μm (Ref 15) and preliminary evidence from gas chromatographic analysis indicates the presence of substantial quantities of methane, this mechanism cannot be the dominant one for the decomposition of MMA. The experimental rate expression (Ref 17)

$$-\frac{d[CH_3NH_2]}{dt} = k[CH_3NH_2]^{.28} \tag{22}$$

differs substantially from the present results, since different experimental conditions were employed and Eq (22) applies to the entire reaction scheme. The present experiment deals with only the first few reaction steps and no valid comparison can be made between the two rate expressions.

A final consideration is pertinent. Since the high pressure activation energy in the present case is substantially lower than the estimated 79 kcal/mole C-N bond strength in MMA (Ref 5) and all other pathways having been eliminated, then it must be taken that a radical chain mechanism is operating. The first step in this radical chain is postulated to be CN bond scissure and the mechanism described by Equations 24 through 29 is taken to be the dominant one for the decomposition of MMA.

Attempts were made to monitor the IR emission at 7.6, 7.3, and 5.23 μm with the HgCdTe detector. Although satisfactory optical alignment was made on the HgCdTe optical system using a glowing coil (Ref 14), no useable oscillograms were obtained during a test. The signal to noise (S/N) ratio for the HgCdTe detector is 3×10^3 which compares favorably with the S/N ratio for the InSb detector of 4×10^3. The detectivity, D*, for the HgCdTe detector is 8×10^9 $cmHz^{\frac{1}{2}}/watt$, whereas D* for the InSb detector is 24×10^9 $cmHz^{\frac{1}{2}}/watt$. This means that the HgCdTe detector is 1/3 as sensitive as the InSb detector. The maximum oscilloscope trace value was 3 mv for any given shot when detected by the InSb detector. According to the specifications supplied by SBRC, the noise level of the HgCdTe detector is 6 mv. Therefore any expected signal from the HgCdTe detector during a test would be completely masked by the noise. Until a more sensitive detector system is obtained, IR observations of this particular reaction will be severely limited at wavelengths longer than 5.5 microns.

VI. Conclusions

As a result of this study the following conclusions are drawn:

1. The high-pressure Arrhenius equation was determined to be

$$k_{uni(P=\infty)} = 10^{10.84} e^{-48,150/RT}$$

2. The decomposition of MMA is unimolecular and the Hinshelwood-Lindemann model is an adequate representation.

3. Ammonia and methane are formed as products in the decomposition of monomethylamine.

4. The rate of disappearance of MMA is twice the rate of formation of ammonia

$$\frac{d[NH_3]}{dt} = -\frac{1}{2}\frac{d[CH_3NH_2]}{dt}$$

5. The dominant reaction pathway is taken to be CN bond scissure followed by the radical chain mechanism as described by Equations 24 through 29.

VII. Recommendations

The following recommendations are made to determine more precisely the mechanism by which monomethylamine decomposes and also to present further areas of interest which should be explored.

1. Single-pulse shock tube studies in conjunction with vapor phase chromatography should be completed on MMA decomposition to determine the product composition.

2. A detector/preamplifier system should be obtained to provide a S/N ratio of 3×10^3 and D* of 24×10^9 or better for the study of the decomposition of MMA in the IR region above 5.5 microns.

3. Shock tube studies should be begun on the decomposition of MMA in an oxygen/argon mixture with an appropriate product analysis to determine the reaction mechanism by which NO_x pollutants are formed.

Bibliography

1. Bauer, S. H. "Chemical Kinetics in Shock Tubes", Science, 141: 867-879 (September 6, 1963).

2. Blazowski, William S. "Research Topics in Turbine Combustion Technology", Fuels and Lubrication Division, Air Force Aero Propulsion Laboratory, Wright-Patterson AFB, Ohio, 1975.

3. Blazowski, William S. "Aircraft Altitude Emissions: Fundamental Concepts and Future R & D Requirements". AIAA Paper 75-1017, AIAA 1975 Aircraft System and Technology Meeting, Los Angeles, California, August 4-7, 1975.

4. Burcat, A., G. Skinner, R. Crossley and K. Scheller. "High Temperature Decomposition of Ethane". International Journal of Chemical Kinetics, V, 345-352 (1973).

5. Chemical Rubber Company. Handbook of Chemistry and Physics (55th Edition). Cleveland, Ohio: 1974.

6. Dzuna, E. R. "Combustion Tests on Shale Oil Fuels". 1976 Spring Technical Meeting of the Central States Section of the Combustion Institute, Columbus, Ohio, April 5-6, 1976.

7. Dorko, E. A., et al. "Shock Tube Isomerization of Cyclopropane". Journal of Chemical Physics, 75: 2526 (1971).

8. Dorko, E. A., et al. "Shock Tube Isomerization of Cyclopropane. II. Investigation of a Vibrationally Excited Intermediate". Journal of Physical Chemistry, 77: 143 (1973).

9. Dorko, E. A., et al. "Shock Tube Decomposition of Dilute Mixtures of Nitrogen Trifluoride in Argon". Journal of Chemical Physics, 63; 3596 (1973).

10. Gray, Peter and J. C. J. Thynne. "Hydrogen and Deuterium Atom Abstraction from Methylamine and Deuterated Methylamines". Trans Faraday Soc, 59: 2275 (1963).

11. Hardin, M. C. "The Combustion of Shale Derived Marine Diesel Fuel at Marine Gas Turbine Engine Conditions". 1976 Spring Technical Meeting of the Central States Section of the Combustion Institute, Columbus, Ohio, April 5-6, 1976.

12. Hidaka, Y., K. Saito, and H. Yamamura. "The Thermal Decomposition of CH_3NH_2 in Shock Waves". Chemistry Letters, 1151 (1973).

13. Meyer, E. and H. Gg. Wagner. "Sum Mechanismus des Thermischen Hydrazingerfalls". Z. Physik Chem Neue Folge, 89: 329 (1974).

14. Pchelkin, Nicholas R. Initial Shock Tube Kinetic Studies of Monomethylamine. GEP/CH/76D-1; Dayton: Air Force Institute of Technology, December, 1976.

15. Pierson, Raymond H., Aaron N. Fletcher, and E. St. Clair Gantz. "Catalog of Infrared Spectra for Qualitative Analysis of Gasses". Analytical Chemistry, 28: 1218 (1956).

16. Robinson, P. T. and K. A. Holbrook. Unimolecular Reactions. London: Wiley-Interscience, 1972.

17. Smith, O. I. and R. F. Sawyer. The Thermal Pyrolysis of Methylamine. UCB-ME-76-2; Berkeley: University of California, April, 1976

18. Stull, D. R., E. F. Westrum, Jr, and G. C. Sinke. The Chemical Thermodynamics of Organic Compounds.

19. Vogt, R. A. and N. M. Laurendeau. "NO_x Formation from Coal Nitrogen: A Review and a Model". 1976 Spring Technical Meeting of the Central States Section of the Combustion Institute, Columbus, Ohio, April 5-6, 1976.

20. Weidman, G. H. and P. M. Utterback. "Liquid Fuel Analyses - Their Effect on Combustion and Emissions". 1976 Spring Technical Meeting of the Central States Section of the Combustion Institute, Columbus, Ohio, April 5-6, 1976.

21. Weston, R. E., Jr and A. A. Schwarz. Chemical Kinetics. Englewood Cliffs, New Jersey: Prentice-Hall, 1972.

APPENDIX A

DERIVATION OF THE RATE EQUATION FOR THE ETHANE ANALOGOUS DECOMPOSITION OF MONOMETHYLAMINE

The postulated reaction steps are

$$CH_3NH_2 \rightarrow CH_3 + NH_2 \quad (1)$$

$$CH_3 + CH_3NH_2 \rightarrow CH_4 + CH_2NH_2 \quad (2)$$

$$CH_2NH_2 \rightarrow CH_2{=}NH + H \quad (3)$$

$$H + CH_3NH_2 \rightarrow H_2 + CH_2NH_2 \quad (4)$$

$$H + CH_3 \rightarrow CH_4 \quad (5)$$

The rate equations for this mechanism are

$$-\frac{d[CH_3NH_2]}{dt} = k_1[CH_3NH_2] + k_2[CH_3NH_2][CH_3] + k_4[CH_3NH_2][H] \quad (6)$$

$$\frac{d[CH_3]}{dt} = k_1[CH_3NH_2] - k_2[CH_3NH_2][CH_3] - k_5[CH_3][H] \quad (7)$$

$$\frac{d[H]}{dt} = k_3[CH_3NH_2] - k_4[H][CH_3NH_2] - k_5[CH_3][H] \quad (8)$$

$$\frac{d[CH_2NH_2]}{dt} = k_2[CH_3][CH_3NH_2] - k_3[CH_2NH_2] + k_4[H][CH_3NH_2] \quad (9)$$

Assuming the steady state approximation for Eq (7) yields Eq (10)

$$k_1[CH_3NH_2] = k_2[CH_3][CH_3NH_2] + k_5[CH_3][H] \quad (10)$$

Solving Eq (10) for $[CH_3]$ yields Eq (11)

$$[CH_3] = \frac{k_1[CH_3NH_2]}{k_2[CH_3NH_2] + k_5[H]} \quad (11)$$

Subtracting Eq (8) from Eq (7) yields Eq (12)

$$k_1[CH_3NH_2] - k_3[CH_2NH_2] - k_2[CH_3][CH_3NH_2] + k_4[H][CH_3NH_2] = 0 \quad (12)$$

Solving Eq (12) for $[CH_2NH_2]$ yields Eq (13)

$$[CH_2NH_2] = [CH_3NH_2]\left(\frac{k_1 - k_2[CH_3] + k_4[H]}{k_3}\right) \quad (13)$$

Assuming the steady state approximation for Eq (9) yields Eq (14)

$$k_3[CH_2NH_2] = k_2[CH_3][CH_3NH_2] + k_4[H][CH_3NH_2] \quad (14)$$

Solving Eq (14) for $[CH_2NH_2]$ yields Eq (15)

$$[CH_2NH_2] = [CH_3NH_2]\left(\frac{k_2[CH_3] + k_4[H]}{k_3}\right) \quad (15)$$

Equating Eq (13) and Eq (15) yields Eq (16)

$$k_1 - k_2[CH_3] + k_4[H] = k_2[CH_3] + k_4[H] \tag{16}$$

Solving Eq (16) for $[CH_3]$ yields Eq (17)

$$[CH_3] = \frac{k_1}{2k_2} \tag{17}$$

Equating Eq (11) and Eq (17) yields Eq (18)

$$\frac{k_1[CH_3NH_2]}{k_2[CH_3NH_2] + k_5[H]} = \frac{k_1}{2k_2} \tag{18}$$

Solving Eq (18) for $[H]$ yields Eq (19)

$$[H] = \frac{k_2}{k_5}[CH_3NH_2] \tag{19}$$

Substituting Eq (19) and Eq (17) into Eq (6) yields Eq (20)

$$-\frac{d[CH_3NH_2]}{dt} = k_1[CH_3NH_2] + k_2[CH_3NH_2]\frac{k_1}{2k_2} + k_4[CH_3NH_2]\frac{k_2}{k_5}[CH_3NH_2] \tag{20}$$

Collecting like terms yields Eq (21)

$$-\frac{d[CH_3NH_2]}{dt} = \frac{3}{2}k_1[CH_3NH_2] + \frac{k_2k_4}{k_5}[CH_3NH_2]^2 \tag{21}$$

APPENDIX B

DERIVATION OF THE RATE EQUATION

FOR

DECOMPOSITION OF MONOMETHYLAMINE

The proposed reaction steps are

$$CH_3NH_2 \rightarrow CH_3 + NH_2 \quad (1)$$

$$CH_3 + CH_3NH_2 \rightarrow CH_4 + CH_2NH_2 \quad (2)$$

$$CH_3 + CH_2NH_2 \rightarrow CH_4 + CH_2{=}NH \quad (3)$$

$$NH_2 + CH_3NH_2 \rightarrow NH_3 + CH_2NH_2 \quad (4)$$

$$NH_2 + CH_2NH_2 \rightarrow NH_3 + CH_2{=}NH \quad (5)$$

$$CH_2{=}NH \rightarrow H_2 + HCN \quad (6)$$

The rate equations for this reaction are

$$-\frac{d[CH_3NH_2]}{dt} = k_1[CH_3NH_2 + k_2[CH_3][CH_3NH_2] + k_4[NH_2][CH_3NH_2] \quad (7)$$

$$\frac{d[CH_3]}{dt} = k_1[CH_3NH_2] - k_2[CH_3NH_2][CH_3] - k_3[CH_3][CH_2NH_2] \quad (8)$$

$$\frac{d[NH_2]}{dt} = k_1[CH_3NH_2] - k_4[NH_2][CH_3NH_2] - k_5[NH_2][CH_2NH_2] \quad (9)$$

$$\frac{d[CH_2NH_2]}{dt} = k_2[CH_3][CH_3NH_2] - k_3[CH_3][CH_2NH_2] + k_4[NH_2][CH_3NH_2] - k_5[NH_2][CH_2NH_2] \quad (10)$$

Assuming the steady state approximation for Eq (10) yields Eq (11)

$$[CH_2NH_2](k_3[CH_3] + k_5[NH_2]) = [CH_3NH_2](k_2[CH_3] + k_4[NH_2]) \quad (11)$$

Solving Eq (11) for $[CH_2NH_2]$ yields Eq (12)

$$[CH_2NH_2] = [CH_3NH_2]\left(\frac{k_2[CH_3] + k_4[NH_2]}{k_3[CH_3] + k_5[NH_2]}\right) \quad (12)$$

Assuming the steady state approximation for Eq (8) yields Eq (13)

$$(k_1 - k_2[CH_3])[CH_3NH_2] = k_3[CH_3][CH_2NH_2] \quad (13)$$

Solving Eq (13) for $[CH_2NH_2]$ and substituting into Eq (12) yields Eq (14)

$$k_1[CH_3NH_2] - k_2[CH_3][CH_3NH_2] - k_3[CH_3][CH_3NH_2]\left(\frac{k_2[CH_3] + k_4[NH_2]}{k_3[CH_3] + k_5[NH_2]}\right) = 0 \quad (14)$$

Solving Eq (14) for k_1 yields Eq (15)

$$k_1 = [CH_3]\left\{k_2 + k_3\left(\frac{k_2[CH_3] + k_4[NH_2]}{k_3[CH_3] + k_5[NH_2]}\right)\right\} \quad (15)$$

Assuming the steady state approximation for Eq (9) yields Eq (16)

$$(k_1 - k_4[NH_2])[CH_3NH_2] = k_5[NH_2][CH_2NH_2] \tag{16}$$

Solving Eq (16) for $[CH_2NH_2]$ and substituting into Eq (12) yields Eq (17)

$$k_1[CH_3NH_2] - k_4[CH_3][CH_3NH_2] - k_5[CH_3][CH_3NH_2]\left(\frac{k_2[CH_3] + k_4[NH_2]}{k_3[CH_3] + k_5[NH_2]}\right) = 0 \tag{17}$$

Solving Eq (17) for k_1 yields Eq (18)

$$k_1 = [NH_2]\left\{k_4 + k_5\left(\frac{k_2[CH_3] + k_4[NH_2]}{k_3[CH_3] + k_5[NH_2]}\right)\right\} \tag{18}$$

Setting Eq (15) equal to Eq (18) yields Eq (19)

$$[CH_3]\left\{k_2 + k_3\left(\frac{k_2[CH_3] + k_4[NH_2]}{k_3[CH_3] + k_5[NH_2]}\right)\right\} = [NH_2]\left\{k_4 + k_5\left(\frac{k_2[CH_3] + k_4[NH_2]}{k_3[CH_3] + k_5[NH_2]}\right)\right\} \tag{19}$$

Expanding Eq (19) and cancelling like terms yields Eq (20)

$$[NH_2] = \beta[CH_3], \text{ where } \beta = \left(\frac{k_2k_3}{k_4k_5}\right)^{\frac{1}{2}} \tag{20}$$

Substituting Eq (20) for $[NH_2]$ into Eq (15) and solving for $[CH_3]$ yields Eq (21)

$$[CH_3] = \frac{k_1k_3 + k_1k_5\beta}{2k_2k_3 + k_2k_5\beta + k_3k_4\beta} \tag{21}$$

Substituting Eq (21) into Eq (20) yields Eq (22)

$$[NH_2] = \left(\frac{k_1k_3 + k_1k_5\beta}{2k_2k_3 + k_2k_5\beta + k_3k_4\beta}\right)\beta \tag{22}$$

Substituting Eq (21) and Eq (22) into Eq (7) yields Eq (23)

$$\frac{-d[CH_3NH_2]}{[CH_3NH_2]} = \left\{k_1 + k_2\left(\frac{k_1k_3 + k_1k_5\beta}{2k_2k_3 + k_2k_5\beta + k_3k_4\beta}\right) + k_4\beta\left(\frac{k_1k_3 + k_1k_5\beta}{2k_2k_3 + k_2k_5\beta + k_3k_4\beta}\right)\right\}dt \tag{23}$$

Expanding Eq (23) and collecting terms yields Eq (24)

$$\frac{-d[CH_3NH_2]}{dt} = 2k_1[CH_3NH_2] \tag{24}$$

APPENDIX C

DERIVATION OF $I_{relative}$ AND THE STOICHIOMETRIC FACTOR α

The generalized rate equations are

$$-\frac{d[CH_3NH_2]}{dt} = k[CH_3NH_2] \quad (1)$$

$$\frac{d[NH_3]}{dt} = k'[CH_3NH_2] \quad (2)$$

The concentration of MMA at any time t is given by Eq (3)

$$[CH_3NH_2] = [CH_3NH_2]_i - \alpha[NH_3] \quad (3)$$

where α is a proportionality constant.

Substituting Eq (3) into Eq (2) yields Eq (4)

$$\frac{d[NH_3]}{dt} = k'([CH_3NH_2]_i - \alpha[NH_3]) \quad (4)$$

Dividing both sides of Eq (4) by $[CH_3NH_2]_i$ yields Eq (5)

$$\frac{d[NH_3]}{dt}\frac{1}{[CH_3NH_2]_i} = k'\left(1 - \frac{\alpha[NH_3]}{[CH_3NH_2]_i}\right) \quad (5)$$

Setting $[CH_3NH_2]_i = \alpha[NH_3]_f$, Eq (5) becomes Eq (6)

$$\frac{d[NH_3]}{dt}\frac{1}{\alpha[NH_3]_f} = k'\left(1 - \frac{\alpha[NH_3]}{\alpha[NH_3]_f}\right) \quad (6)$$

Rearranging Eq (6) yields Eq (7)

$$\frac{d[NH_3]}{dt}\frac{1}{[NH_3]_f} = \alpha k'\left(1 - \frac{[NH_3]}{[NH_3]_f}\right) \quad (7)$$

Since the intensity of emission is directly proportional to the concentration (Ref 8)

$$\left(1 - \frac{[NH_3]}{[NH_3]_f}\right) = I_{rel} = \frac{I_{max} - I_{measured}}{I_{max}}$$

Substituting Eq (3) into Eq (1) yields Eq (8)

$$-\frac{d[CH_3NH_2]}{dt} = k([CH_3NH_2]_i - \alpha[NH_3]) \quad (8)$$

Dividing both sides of Eq (8) by $[CH_3NH_2]_i$ yields Eq (9)

$$-\frac{d[CH_3NH_2]}{dt}\frac{1}{[CH_3NH_2]_i} = k\left(1 - \frac{\alpha[NH_3]}{[CH_3NH_2]_i}\right) \quad (9)$$

Setting $[CH_3NH_2]_i = \alpha[NH_3]_f$, Eq (9) becomes Eq (10)

$$-\frac{d[CH_3NH_2]}{dt}\frac{1}{[CH_3NH_2]_i} = k\left(1 - \frac{\alpha[NH_3]}{\alpha[NH_3]_f}\right) \tag{10}$$

Rearranging Eq (10) yields Eq (11)

$$-\frac{d[CH_3NH_2]}{dt}\frac{1}{[CH_3NH_2]_i} = k\left(1 - \frac{[NH_3]}{[NH_3]_f}\right) \tag{11}$$

Equating Eq (11) and Eq (7) yields Eq (12)

$$k\left(1 - \frac{[NH_3]}{[NH_3]_f}\right) = \alpha k'\left(1 - \frac{[NH_3]}{[NH_3]_f}\right) \tag{12}$$

Cancelling like terms yields Eq (13)

$$k = \alpha k' \quad \text{or} \quad \alpha = \frac{k}{k'} \tag{13}$$

APPENDIX D

DERIVATION OF THE RATE EQUATION

FOR

FORMATION OF AMMONIA

Using the equations from Appendix B, the derivation of the rate equation for the formation of NH_3 follows. The equations from Appendix B will be designated by an asterisk (*).

The rate equation for the formation of NH_3 is

$$\frac{d[NH_3]}{dt} = k_4[NH_2][CH_3NH_2] + k_5[NH_2][CH_2NH_2] \tag{1}$$

Substituting Eq (12*) into Eq (1) yields Eq (2)

$$\frac{d[NH_3]}{dt} = k_4[NH_2][CH_3NH_2] + k_5[NH_2][CH_3NH_2]\left(\frac{k_2[CH_3] + k_4\beta[CH_3]}{k_3[CH_3] + k_5\beta[CH_3]}\right) \tag{2}$$

Substituting Eq (20*) into Eq (2) yields Eq (3)

$$\frac{d[NH_3]}{dt} = k_4\beta[CH_3][CH_3NH_2] + k_5\beta[CH_3][CH_3NH_2]\left(\frac{k_2[CH_3] + k_4\beta[CH_3]}{k_3[CH_3] + k_5\beta[CH_3]}\right) \tag{3}$$

Collecting like terms yields Eq (4)

$$\frac{d[NH_3]}{dt} = [CH_3][CH_3NH_2]\left\{k_4\beta + \beta k_5\left(\frac{k_2 + k_4\beta}{k_3 + k_5\beta}\right)\right\} \tag{4}$$

Substituting Eq (21*) into Eq (4) yields Eq (5)

$$\frac{d[NH_3]}{dt} = [CH_3NH_2]\left(\frac{k_1k_3 + k_1k_5\beta}{2k_2k_3 + k_2k_5\beta + k_3k_4\beta}\right)\left\{k_4\beta + k_5\beta\left(\frac{k_2 + k_4\beta}{k_3 + k_5\beta}\right)\right\} \tag{5}$$

Expanding Eq (5) and cancelling like terms yields Eq (6)

$$\frac{d[NH_3]}{dt} = k_1[CH_3NH_2] \tag{6}$$

Restating Eq (24*) yields Eq (7)

$$-\frac{1}{2}\frac{d[CH_3NH_2]}{dt} = k_1[CH_3NH_2] \tag{7}$$

Equating Eq (6) and Eq (7) yields Eq (8)

$$\frac{d[NH_3]}{dt} = -\frac{1}{2}\frac{d[CH_3NH_2]}{dt} \tag{8}$$

APPENDIX E

CALCULATION OF THE HEAT OF FORMATION OF CH_2=NH

An estimate of the heat of fomation of CH_2=NH was determined in the following manner. All values are in kcal/mole. The heat of formation for CH_2=CH_2 lies between the heat of formation for CH_3-CH_3 and CH≡CH.

Calculated: $$\Delta H_{f(CH_2=CH_2)} = \frac{\Delta H_{f(CH_3-CH_3)} + \Delta H_{f(CH\equiv CH)}}{2} = 16.979$$

Actual: $$\Delta H_{f(CH_2=CH_2)} = 12.496$$

$$\delta_{(CH_2=CH_2)} = \Delta H_{f(calculated)} - \Delta H_{f(actual)} = 4.483$$

The heat of formation for CH_2=NH should lie between CH_3-NH_2 and HC≡N.

Calculated: $$\Delta H_{f(CH_2=NH)} = \frac{\Delta H_{f(CH_3-CH_3)} + \Delta H_{f(HC\equiv N)}}{2} = 12.25$$

The actual value is unknown, therefore the following approximation was used to compute the difference between the calculated and "actual" value.

$$\delta_{(CH_2=NH)} \approx \delta_{(CH_2=CH_2)}\left(\frac{\Delta H_{f(CH_2=NH)calculated}}{\Delta H_{f(CH_2=CH_2)calculated}}\right) = 3.23$$

"Actual": $$\Delta H_{f(CH_2=NH)} = \Delta H_{f(CH_2=NH)calculated} - \delta_{(CH_2=NH)} = 9.02$$

APPENDIX F

EXPERIMENTAL DATA

1/T VS K UNI M = 15.32 MICROMOL/CC
MMA DECOMPOSITION

TOTAL ROOT MEAN SQUARE RESIDUE= .1502908E-01
BEST POLYN OF DEGREE 1FOR , 16DATA PTS IS

	COEFFICIENT	POWER OF X
LOG Y =	.9266158405E+01	0
	-.8913122051E+04	1

CORRELATION COEFFICIENT = -.983

TEMP	LOG K UNI
.1911000E+04	.3935000E+01
.1895000E+04	.3666000E+01
.1888000E+04	.3615000E+01
.1884000E+04	.3435000E+01
.1883000E+04	.3516000E+01
.1882000E+04	.3304000E+01
.1853000E+04	.2959000E+01
.1848000E+04	.2743000E+01
.1845000E+04	.2795000E+01
.1841000E+04	.2414000E+01
.1838000E+04	.2725000E+01
.1836000E+04	.2488000E+01
.1829000E+04	.2443000E+01
.1827000E+04	.2390000E+01
.1815000E+04	.2335000E+01
.1795000E+04	.2036000E+01

1/T VS K UNI M = 27.50 MICROMOL/CC
MMA DECOMPOSITION

TOTAL ROOT MEAN SQUARE RESIDUE= .5474549E-01
BEST POLYN OF DEGREE 1FOR , 18DATA PTS IS

	COEFFICIENT	POWER OF X
LOG Y =	.9480905[illegible]E+01	0
	-.8996472902E+04	1

CORRELATION COEFFICIENT = -.995

TEMP	LOG K UNI
.1961000E+04	.3499000E+01
.1858000E+04	.3738000E+01
.1854000E+04	.3595000E+01
.1843000E+04	.4539000E+01
.1756000E+04	.2496000E+01
.1749000E+04	.2511000E+01
.1740000E+04	.1974000E+01
.1737000E+04	.2211000E+01
.1703000E+04	.1933000E+01
.1683000E+04	.1415000E+01
.1579000E+04	.6454000E+00
.1551000E+04	.5480000E+00
.1489000E+04	.2877000E+00
.1484000E+04	.2479000E+00
.1454000E+04	.1507000E+00
.1453000E+04	.1684000E+00
.1445000E+04	.2007000E+00
.1435000E+04	.1589000E+00

1/T VS K UNI M = 53.04 MICROMOL/CC
MMA DECOMPOSITION

TOTAL ROOT MEAN SQUARE RESIDUE= .3627890E-01
BEST POLYN OF DEGREE 1FOR , 20DATA PTS IS

	COEFFICIENT	POWER OF X
LOG Y =	.1020147683E+02	0
	-.9807948196E+04	1

CORRELATION COEFFICIENT = -.993

TEMP	LOG K UNI
.1759000E+04	.4229000E+01
.1738000E+04	.3447000E+01
.1735000E+04	.3198000E+01
.1674000E+04	.1983000E+01
.1669000E+04	.2283000E+01
.1664000E+04	.2347000E+01
.1653000E+04	.1980000E+01
.1630000E+04	.1531000E+01
.1614000E+04	.1348000E+01
.1569000E+04	.9455000E+00
.1567000E+04	.8925000E+00
.1546000E+04	.6559000E+00
.1524000E+04	.6624000E+00
.1518000E+04	.5789000E+00
.1518000E+04	.5970000E+00
.1512000E+04	.5650000E+00
.1510000E+04	.4614000E+00
.1495000E+04	.4454000E+00
.1471000E+04	.3264000E+00
.1407000E+04	.1428000E+00

1/T VS K UNI @ M = 83.73 MICROMOL/CC
MMA DECOMPOSITION

TOTAL ROOT MEAN SQUARE RESIDUE= .3099170E-01
BEST POLYN OF DEGREE 1FOR , 14DATA PTS IS

	COEFFICIENT	POWER OF X
LOG Y =	.1062104479E+02	0
	-.1028725975E+05	1

CORRELATION COEFFICIENT = -.996

TEMP	LOG K UNI
.1711000E+04	.3834000E+01
.1651000E+04	.2417000E+01
.1618000E+04	.1805000E+01
.1616000E+04	.1903000E+01
.1577000E+04	.1238000E+01
.1549000E+04	.1055000E+01
.1548000E+04	.1033000E+01
.1534000E+04	.8273000E+00
.1478000E+04	.4701000E+00
.1473000E+04	.3683000E+00
.1467000E+04	.3921000E+00
.1463000E+04	.3655000E+00
.1457000E+04	.3676000E+00
.1425000E+04	.2784000E+00

1/T VS K UNI M = 114.7 MICROMOL/CC
MMA DECOMPOSITION

TOTAL ROOT MEAN SQUARE RESIDUE= .1467154E-01
BEST POLYN OF DEGREE 1FOR', 13DATA PTS IS

	COEFFICIENT	POWER OF X
LOG Y =	.1070424461E+02	0
	-.1035546410E+05	1

CORRELATION COEFFICIENT = -.998

TEMP	LOG K UNI
.1578000E+04	.1299000E+01
.1515000E+04	.7821000E+00
.1514000E+04	.7558000E+00
.1496000E+04	.6080000E+00
.1457000E+04	.3943000E+00
.1454000E+04	.3872000E+00
.1441000E+04	.3270000E+00
.1436000E+04	.3195000E+00
.1433000E+04	.2965000E+00
.1416000E+04	.2428000E+00
.1413000E+04	.2385000E+00
.1407000E+04	.2275000E+00
.1404000E+04	.1997000E+00

1/T VS K UNI M = 27.50 MICROMOL/CC
AMMONIA FORMATION

TOTAL ROOT MEAN SQUARE RESIDUE= .3657182E-01

BEST POLYN OF DEGREE 1FOR , 12DATA PTS IS

	COEFFICIENT	POWER OF X
LOG Y =	.9275452476E+01	0
	-.8905727910E+04	1

CORRELATION COEFFICIENT = -.984

TEMP	LOG K UNI
.1898000E+04	.4160000E+01
.1864000E+04	.3220000E+01
.1863000E+04	.3140000E+01
.1835000E+04	.2570000E+01
.1834000E+04	.2390000E+01
.1769000E+04	.1800000E+01
.1749000E+04	.1390000E+01
.1732000E+04	.1490000E+01
.1719000E+04	.1060000E+01
.1703000E+04	.1120000E+01
.1703000E+04	.1100000E+01
.1696000E+04	.1070000E+01

1/T VS K UNI M = 53.04 MICROMOL/CC
AMMONIA FORMATION

TOTAL ROOT MEAN SQUARE RESIDUE= .4713096E-01
BEST POLYN OF DEGREE 1FOR , 18DATA PTS IS

	COEFFICIENT	POWER OF X
LOG Y =	.9868101073E+01	0
	-.9734772073E+04	1

CORRELATION COEFFICIENT = -.983

TEMP	LOG K UNI
.1770000E+04	.2204000E+01
.1722000E+04	.1605000E+01
.1698000E+04	.1130000E+01
.1686000E+04	.1350000E+01
.1678000E+04	.1100000E+01
.1675000E+04	.1170000E+01
.1669000E+04	.1204000E+01
.1668000E+04	.9920000E+00
.1656000E+04	.1030000E+01
.1635000E+04	.9400000E+00
.1617000E+04	.8260000E+00
.1613000E+04	.7900000E+00
.1602000E+04	.5160000E+00
.1592000E+04	.4570000E+00
.1575000E+04	.4700000E+00
.1554000E+04	.4550000E+00
.1551000E+04	.3720000E+00
.1479000E+04	.1880000E+00

1/T VS K UNI M = 83.73 MICROMOL/CC
AMMONIA FORMATION

TOTAL ROOT MEAN SQUARE RESIDUE= .3792114E-01
BEST POLYN OF DEGREE 1FOR , 17DATA PTS IS

	COEFFICIENT	POWER OF X
LOG Y =	.1037201030E+02	0
	-.1015849519E+05	1

CORRELATION COEFFICIENT = -.990

TEMP	LOG K UNI
.1693000E+04	.2139000E+01
.1638000E+04	.2183000E+01
.1662000E+04	.1720000E+01
.1659000E+04	.1998000E+01
.1652000E+04	.1815000E+01
.1647000E+04	.1791000E+01
.1587000E+04	.6870000E+00
.1577000E+04	.8330000E+00
.1573000E+04	.7790000E+00
.1565000E+04	.6390000E+00
.1557000E+04	.6910000E+00
.1554000E+04	.7470000E+00
.1545000E+04	.6980000E+00
.1515000E+04	.4350000E+00
.1501000E+04	.3930000E+00
.1498000E+04	.3690000E+00
.1493000E+04	.4210000E+00

VITA

John C. Wert III was born in Jersey City, New Jersey on 20 Dec 1942. He graduated from high school in Rockaway, New Jersey in 1961 and enlisted in the Air Force. After four years of active duty, he remained in the Air Force Reserve and attended the University of North Carolina-Asheville. He received the degree of Bachelor of Arts in Chemistry and Physics in 1969. After graduation he entered Air Force Officer Training School and was commissioned in December 1969. He served as a Deputy Missile Combat Crew Commander in the 571st Strategic Missile Squadron and as a Missile Combat Crew Commander in the 570th Strategic Missile Squadron, Davis-Monthan AFB, Arizona. He then served as a Missile Maintenance Officer with the 390th Missile Maintenance Squadron at Davis-Monthan AFB until entering the School of Engineering, Air Force Institute of Technology, in May 1975.

Permanent Address: 763 Tamerlane
Deltona, Florida 32763

UNCLASSIFIED

SECURITY CLASSIFICATION OF THIS PAGE (When Data Entered)

REPORT DOCUMENTATION PAGE

READ INSTRUCTIONS BEFORE COMPLETING FORM

1. REPORT NUMBER: AFIT/CEP/AA/77D-1	2. GOVT ACCESSION NO. (9) Master's thesis
4. TITLE (and Subtitle): (6) FURTHER SHOCK TUBE KINETIC STUDIES OF MONOMETHYLAMINE,	5. TYPE OF REPORT & PERIOD COVERED: MS THESIS
	6. PERFORMING ORG. REPORT NUMBER
7. AUTHOR(s): (10) John C. Wert, III, Captain, USAF	8. CONTRACT OR GRANT NUMBER(s): (17) 00
9. PERFORMING ORGANIZATION NAME AND ADDRESS: Air Force Institute of Technology (AFIT-EN) Wright-Patterson AFB, Ohio 45433	10. PROGRAM ELEMENT, PROJECT, TASK AREA & WORK UNIT NUMBERS: Project 7071-00-12 (16) 61102F
11. CONTROLLING OFFICE NAME AND ADDRESS (11)	12. REPORT DATE: Dec 77
	13. NUMBER OF PAGES: (12) 69 p.
14. MONITORING AGENCY NAME & ADDRESS(if different from Controlling Office)	15. SECURITY CLASS. (of this report): Unclassified
	15a. DECLASSIFICATION/DOWNGRADING SCHEDULE

16. DISTRIBUTION STATEMENT (of this Report)

Approved for public release; distribution unlimited

17. DISTRIBUTION STATEMENT (of the abstract entered in Block 20, if different from Report)

18. SUPPLEMENTARY NOTES

Approved for public release IAW AFR 190-17

JERRAL F. GUESS, Captain, USAF
Director of Information

19. KEY WORDS (Continue on reverse side if necessary and identify by block number)

micrometers

Shock Tube	Mission
Methylamine	Infrared Radiation
Reaction Kinetics	Pollutants

20. ABSTRACT (Continue on reverse side if necessary and identify by block number)

The pyrolytic decomposition of monomethylamine was studied as a first step toward modeling the route by which NO_x pollutants are formed from nitrogen rich compounds such as coal and shale oil. The decomposition of dilute mixtures of monomethylamine in argon was accomplished using shock tube techniques. Kinetic measurements for the decomposition occurring behind the reflected shock were made by means of infrared measurements. Emissions at 3.375 (μm) due to monomethylamine and 2.886 (μm) due to ammonia were observed. The total gas concentration behind the reflected shock ranged from 15.32 to 114.7 micromoles/cc. The CONT'D

DD FORM 1 JAN 73 1473 EDITION OF 1 NOV 65 IS OBSOLETE

UNCLASSIFIED

SECURITY CLASSIFICATION OF THIS PAGE (When Data Entered)

micrometers

Ø12225

Ltr

20. Abstract(Continued)

temperature range was 1275 to 2400 °K and the total pressure ranged from 1 to 10 atmospheres. The values for the Arrhenius parameters for the decomposition of monomethylamine and the formation of ammonia were determined using a least squares analysis. The high pressure Arrhenius expression for the decomposition is $k = 10^{10.84} e^{-48,150/RT}$. It was discovered that the rate of ammonia formation was one-half the rate of monomethylamine decomposition. The most probable reaction mechanism was determined to be C-N bond scissure followed by a radical chain to produce ammonia, methane, hydrogen cyanide, and hydrogen.

10 to the power 10.84 times exp(-48,150/RT)